Zhiyong Ma
School of Energy, Power and Mechanical Engineering,
North China Electric Power University,
Beijing 102206, China

Yibing Liu
School of Energy, Power and Mechanical Engineering,
North China Electric Power University,
Beijing 102206, China;
Key Laboratory of Condition Monitoring and Control for Power Plant Equipment of Ministry of Education,
North China Electric Power University,
Beijing 102206, China

Dameng Wang
School of Energy, Power and Mechanical Engineering,
North China Electric Power University,
Beijing 102206, China

Wei Teng[1]
School of Energy, Power and Mechanical Engineering,
North China Electric Power University,
Beijing 102206, China;
Key Laboratory of Condition Monitoring and Control for Power Plant Equipment of Ministry of Education,
North China Electric Power University,
Beijing 102206, China
e-mail: tengw_ncepu@163.com

Andrew Kusiak
Mechanical and Industrial Engineering,
3131 Seamans Center,
The University of Iowa,
Iowa City, IA 52242-1527

Cyclostationary Analysis of a Faulty Bearing in the Wind Turbine

Bearing faults occur frequently in wind turbines, thus resulting in an unplanned downtime and economic loss. Vibration signal collected from a failing bearing exhibits modulation phenomenon and "cyclostationarity." In this paper, the cyclostationary analysis is utilized to the vibration signal from the drive-end of the wind turbine generator. Fault features of the inner and outer race become visible in the frequency–cyclic frequency plane. Such fault signatures can not be produced by the traditional demodulation methods. Analysis results demonstrate effectiveness of the cyclostatonary analysis. The disassembled faulty bearing visualizes the fault. [DOI: 10.1115/1.4035846]

Keywords: bearing fault detection, wind turbine generator, cyclostationarity, fault analysis

1 Introduction

The rapid expansion of wind energy has elevated the importance of reliability of wind turbines. To guarantee power quality and reduce maintenance cost, health monitoring systems have been introduced for monitoring conditions of critical subassemblies of wind turbines and diagnosing faults [1–3].

Bearings support revolving shafts in the gearbox and generator of a wind turbine. The bearing at the drive-end of the generator is the most fragile [4,5] as it is affected by the alternating loads caused by the fluctuation of power, shaft corrosion, and the electromagnetic excitation. In addition of these factors, any misalignment between the high speed shaft of a gearbox and the generator shaft may lead to the bearing failure. Shaft misalignment is usually caused by temperature variation or looseness of the foundation bolt.

Different approaches have been developed to detect bearing faults in wind turbines. Watson et al. [6] applied wavelets to analyze the frequency components of the power series. They derived fault characteristics of the generator bearing. Kusiak and Verma [7] used historical temperature measurements to develop a neural network model predicting over-temperature faults of a bearing. Yang et al. [8] established a relationship between the bearing temperature and active power, and derived a fitting coefficient describing different fault levels. The cited above results have been derived based on the data collected by the supervisory control and data acquisition (SCADA) system, thus, avoiding additional hardware and software cost associated with the need to collect vibration data. However, the SCADA data does not suffice to locate a concrete bearing fault.

To date, vibration analysis remains the primary method to diagnose bearing faults. The cost of the acquisition system is compensated by the ease of fault analysis. Using vibration data, Antoni and Randall [9] determined the optimal demodulation frequency band of a faulty bearing with spectral kurtosis. Autoregressive model and minimum entropy deconvolution can restrain the periodic components from the gear mesh and background noise [10,11]. Both were adopted to evidence the impacts of fault bearing in a vibration signal. Randall et al. [12] presented cepstrum prewhitening to eliminate the deterministic components in the cepstrum domain, and applied it to diagnose bearing faults under variable speed conditions [13]. Rai and Mohanty [14] used the

[1]Corresponding author.

Contributed by the Solar Energy Division of ASME for publication in the Journal of Solar Energy Engineering: Including Wind Energy and Building Energy Conservation. Manuscript received December 11, 2016; final manuscript received January 13, 2017; published online February 8, 2017. Assoc. Editor: Yves Gagnon.

fast Fourier transform (FFT) and the Hilbert–Huang transform (HHT) to demonstrate a bearing fault using the nonstationary properties of HHT. Park et al. [15] proposed the minimum variance-based cepstrum for early fault detection in automotive ball bearings. Teng et al. [16] utilized the complex Morlet wavelet to demodulate vibration signals from the direct drive wind turbine and detect roller defects of the rear bearing.

The emerging bearing fault reflects itself in the modulation phenomenon known as the second-order cyclostationarity [17,18]. Therefore, the second-order cyclostationary analysis is regarded as an effective tool for processing the vibration signal associated with a bearing fault. Gardner [19–21] described the foundation of cyclostationary analysis, and proposed important concepts such as spectral correlation and spectral redundancy. Antoni [22–24] adopted the theory of cyclostationary analysis to fault diagnosis of mechanical systems, e.g., a diesel engine, a hydraulic pump, and a gearbox.

To arrive at pure cyclostationarity, Raad et al. [25] computed high order cyclic cumulants, thus, excluding the interference from lower order statistics. However, computing cyclic cumulants is time-consuming for a long data series. The vibration signals from faulty bearing in wind turbine generator represent second-order cyclostationarity, which was not considered in the past research on diagnostic of wind turbines [26,27]. The moment-based cyclostationary analysis can detect this cyclostationarity caused by faulty bearing, and it is highly efficient. In this paper, the cyclostationary analysis based on cyclic moment is applied to analyze the vibration signal originated from a faulty bearing located at the drive-end of a generator. In Sec. 2, the structure of a wind turbine drive train is described, the offline vibration monitoring system is introduced, and the fault feature frequencies are discussed. In Sec. 3, the theoretical aspects of cyclostationary analysis are referred. An operating 1.5 MW generator with a faulty bearing is tested and analyzed in Sec. 4. The disassembled bearing visualizes the bearing fault. Section 5 concludes the paper.

2 Wind Turbine Generator

2.1 Wind Turbine Drive Train. Wind turbines fall into two categories: direct-drive turbines (DDT) and turbines with gearboxes. The direct-drive turbines use full energy conversion produced by synchronous generators. The turbine equipped with a gearbox (see Fig. 1) usually uses a double-fed induction generator (DFIG). Such generator calls for partial energy conversion. The bearing at the drive-end of the generator is prone to failures due to a misalignment between the generator shaft and the high-speed shaft of the gearbox, shaft imbalance, or the distortion due to thermal expansion.

Vibration analysis is frequently applied in the detection of gear and bearing faults. There are seven acceleration transducers installed at the drive train of the wind turbine in Fig. 1. Transducer 1 monitors the blades and the front main bearing. Transducers 2 through 7 sense the signal from the rear main bearing, planetary stage, intermediate stage, high speed stage of gearbox, bearing at drive-end, and bearing at the non-drive-end of the generator, respectively. In this paper, the vibration signal from transducer 6 will be analyzed and discussed.

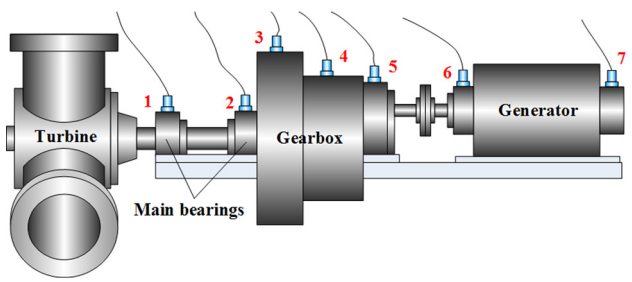

Fig. 1 Structure of wind turbine drive train

2.2 Bearing Fault Features. Rolling bearing is a rotating subassembly composed of an inner race, outer race, rolling elements, and a cage. Due to the relative rotation between the rolling elements and other parts, a bearing defect generates periodic impulses. When a fault arises on the inner race of a bearing, the frequency of the impulses from the balls and the inner race is called the ball pass frequency of inner race (BPFI). Similarly, the frequency of the impulses from the balls and the faulty outer race is called the ball pass frequency of outer race (BPFO), the frequency caused by the faulty ball striking other parts is called ball spin frequency of rolling element (BSF), the frequency of the impulses from the balls and the faulty cage is called fundamental train frequency (FTF). BPFI, BPFO, BSF, and FTF are computed from expressions (1)–(4), respectively [16,24]

$$\mathrm{BPFI} = \frac{f_r N_\mathrm{b}}{2}\left(1 + \frac{d}{D}\cos\varphi\right) \tag{1}$$

$$\mathrm{BPFO} = \frac{f_r N_\mathrm{b}}{2}\left(1 - \frac{d}{D}\cos\varphi\right) \tag{2}$$

$$\mathrm{BSF} = \frac{f_r D}{2d}\left(1 - \left(\frac{d}{D}\cos\varphi\right)^2\right) \tag{3}$$

$$\mathrm{FTF} = \frac{f_r}{2}\left(1 - \frac{d}{D}\cos\varphi\right) \tag{4}$$

where f_r is the rotational frequency of the shaft assembled with inner race, d is the ball diameter, D is the pitch diameter, N_b is the number of the balls, and φ is the bearing contact angle; φ is the angle between the normal through the contact points and the line perpendicular to the axis line of the bearing. The structure of ball bearings is shown in Fig. 2.

3 Cyclostationary Analysis

If the statistics of vibration signal $x(t)$ are periodic, $x(t)$ is regarded as cyclostationary. Take the nth-moment $M_{nx}(t, \tau_1, \ldots, \tau_{n-1}) = \mathrm{E}\{x(t)x(t-\tau_1)\ldots\infty x(t-\tau_{n-1})\}$ with a cyclic period T

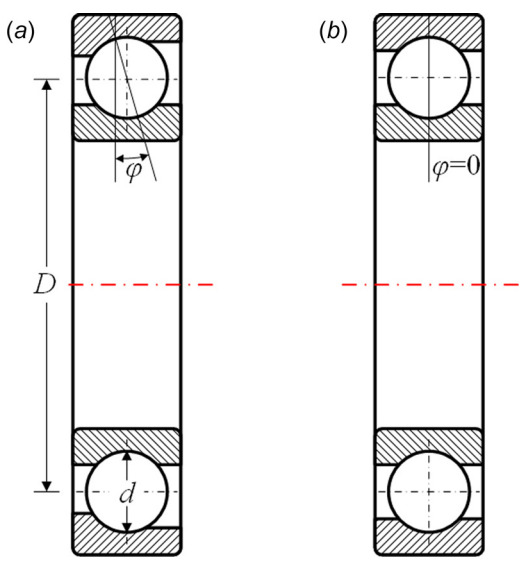

Fig. 2 Structure of ball bearings: (*a*) angular contact ball bearing and (*b*) deep groove ball bearing

for an example, it can be expressed in the cyclic frequency domain as the Fourier series [25] in the below equation

$$M_{nx}(t,\tau_1,\ldots,\tau_{n-1}) = \sum_{\alpha} M_{nx}^{\alpha}(\tau_1,\ldots,\tau_{n-1})\, e^{j2\pi\alpha t} \tag{5}$$

where α is defined as cyclic frequency, $\tau_1,\ldots,\tau_{n-1}$ are time lags and $M_{nx}^{\alpha}(\tau_1,\ldots,\tau_{n-1})$ is nth-order cyclic moments. At different orders, they are expressed in Eqs. (6)–(9)

$$M_{1x}^{\alpha} = \lim_{T\to\infty}\frac{1}{T}\int_{-\frac{T}{2}}^{\frac{T}{2}} M_{1x}(t)e^{-j2\pi\alpha t}dt \tag{6}$$

$$M_{2x}^{\alpha}(\tau) = \lim_{T\to\infty}\frac{1}{T}\int_{-\frac{T}{2}}^{\frac{T}{2}} M_{2x}(t,\tau)e^{-j2\pi\alpha t}dt \tag{7}$$

$$M_{3x}^{\alpha}(\tau_1,\tau_2) = \lim_{T\to\infty}\frac{1}{T}\int_{-\frac{T}{2}}^{\frac{T}{2}} M_{3x}(t,\tau_1,\tau_2)e^{-j2\pi\alpha t}dt \tag{8}$$

$$M_{4x}^{\alpha}(\tau_1,\tau_2,\tau_3) = \lim_{T\to\infty}\frac{1}{T}\int_{-\frac{T}{2}}^{\frac{T}{2}} M_{4x}(t,\tau_1,\tau_2,\tau_3)e^{-j2\pi\alpha t}dt \tag{9}$$

Gears and bearings are symmetric, and therefore, their vibration signal exhibits the first-order cyclostationary characteristic. Moreover, once a gear or a bearing becomes affected by a fault, there are inevitable modulation components in the vibration signal whose second-order moment is periodic [17,18]. Therefore, the second-order cyclostationary analysis is useful in the detection of gear and bearing faults.

The second-order instantaneous moment of the vibration signal, also called the instantaneous auto-correlation function with symmetry structure is defined in the below equation

$$M_{2x}(t,\tau) = E\left\{x\left(t+\frac{\tau}{2}\right)x^*\left(t-\frac{\tau}{2}\right)\right\} \tag{10}$$

where τ is time lag, and x^* is the complex conjugate of x. Substituting the expectation operation in expression (10) with the mean value during the finite sampling range T, the second-order cyclic moment in expression (7) can be rewritten as shown in the below equation

$$\begin{aligned} M_{2x}^{\alpha}(\tau) &= \lim_{T\to\infty}\frac{1}{T}\int_{-\frac{T}{2}}^{\frac{T}{2}} x\left(t+\frac{\tau}{2}\right)x^*\left(t-\frac{\tau}{2}\right)e^{-j2\pi\alpha t}dt \\ &= \left\langle x\left(t+\frac{\tau}{2}\right)x^*\left(t-\frac{\tau}{2}\right)e^{-j2\pi\alpha t}\right\rangle_t \end{aligned} \tag{11}$$

where the $\langle\rangle_t$ denotes the inner product operation. The second-order cyclic moment above can be transformed to the cyclic spectrum density using Fourier transform in the frequency domain as shown in the below equation

$$S_{2x}^{\alpha}(f) = \int_{-\infty}^{\infty} M_{2x}^{\alpha}(\tau)e^{-j2\pi f\tau}d\tau \tag{12}$$

To estimate the cyclic spectrum density using finite time series, the second-order cyclic moment [28] is rewritten according to the below equation

$$M_{2x}^{\alpha}(\tau) = \left\langle u\left(t+\frac{\tau}{2}\right)v^*\left(t-\frac{\tau}{2}\right)\right\rangle_t \tag{13}$$

where

$$\begin{cases} u(t) = x(t)e^{-j\pi\alpha t} \\ v(t) = x(t)e^{j\pi\alpha t} \end{cases} \tag{14}$$

The relationship between the correlation function and convolution [28] is shown in the below equation

$$M_{2x}^{\alpha}(\tau) = u(\tau) * v(-\tau) \tag{15}$$

where * denotes the convolution operator. Therefore, the cyclic spectrum density can be estimated from the below equation

$$S_{2x}^{\alpha}(f) = \lim_{T\to\infty}\frac{U(f)\cdot V^*(f)}{T} \tag{16}$$

where

$$\begin{cases} U(f) = F[u(t)] = X\left(f+\dfrac{\alpha}{2}\right) \\ V(f) = F[v(t)] = X\left(f-\dfrac{\alpha}{2}\right) \end{cases} \tag{17}$$

$V^*(f)$ is the conjugate of $V(f)$; F denotes the Fourier transform operator; and $X(f)$ is the Fourier transform of $x(t)$.

The cyclic coherence function (CCF) that measures the strength of cyclostationarity at cyclic frequency [23] is defined in the below equation

$$C_{2x}^{\alpha}(f) = \frac{U(f)\cdot V^*(f)}{\sqrt{U^2(f)\cdot V^2(f)}} \tag{18}$$

The structure of the second-order cyclic moment in expression (11) is similar to the short time Fourier transform (STFT) if the auto-correlation function is substituted by a windowed signal, and cyclic frequency α is substituted by frequency f. The STFT [29] is defined in the below equation

$$\mathrm{STFT}(\tau,f) = \int_{-\infty}^{\infty} x(t)h^*(t-\tau)e^{-j2\pi ft}dt \tag{19}$$

As a variant of Fourier transform, STFT is invented to analyze nonstationary signal whose frequency varies in a short time. It is troublesome for STFT to reveal the fault information because the fault frequency is usually convoluted by carrier frequency. Moreover, the frequency resolution in STFT is rough due to the handful of data in a windowed signal. By contrast, the second-order cyclic moment in expression (11) can obtain the cyclostationarity of faulty bearing directly through computing the Fourier transform of auto-correlation function in cyclic domain.

4 Case Study

4.1 Testing Conditions. The rated power of the wind turbine studied in this research is 1.5 MW. The corresponding rotational frequency of the generator is of about 30 Hz. The offline vibration analysis was performed twice a year on the turbine. Two different testing conditions were adopted. At condition C1, the rotational frequency of the generator was 28.13 Hz, and the frequency was 24.84 Hz at C2 when the test was carried on 6 months earlier. The sampling frequency was 25,600 Hz. The damaged bearing at the drive-end of the generator was 6330 C3 SKF. According to

Table 1 Bearing feature frequencies at the drive-end of the generator

	f_r	FTF	BSF	BPFO	BPFI
Ratio to f_r	1	0.399	2.37	3.59	5.41
Feature frequency at C1	28.13	11.22	66.67	100.98	152.18
Feature frequency at C2 (6 months earlier)	24.84	9.91	58.87	89.17	134.38

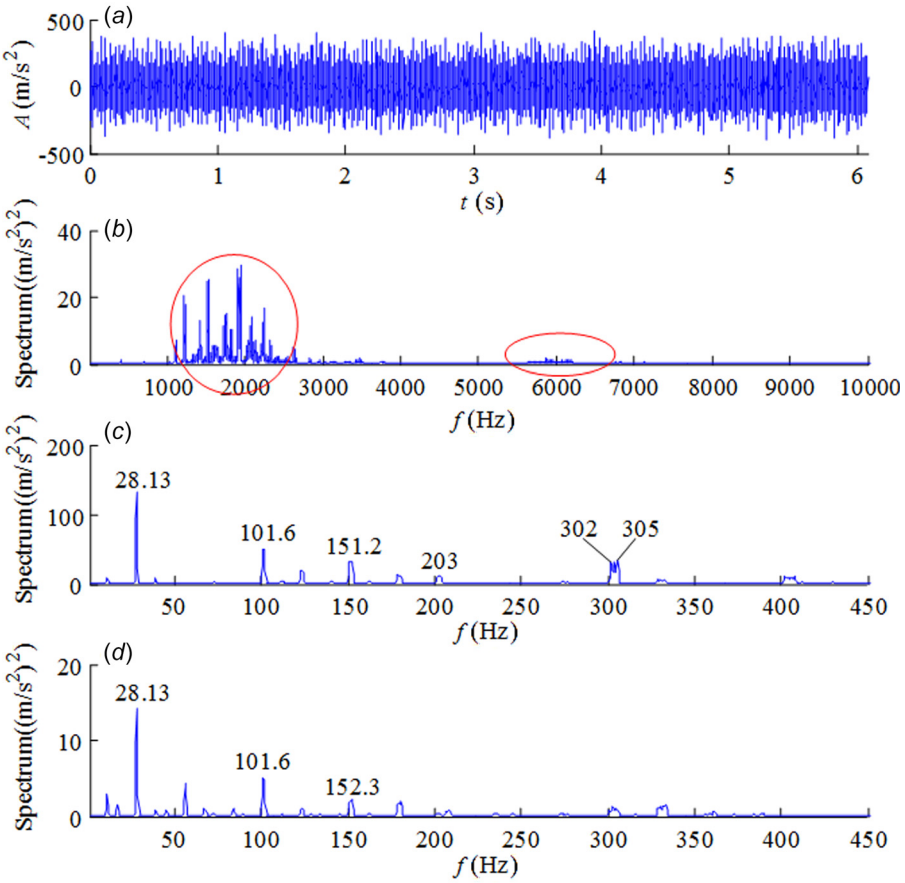

Fig. 3 Time signal at the drive-end of a generator: (*a*) time signal, (*b*) power spectrum, (*c*) envelope spectrum in the band 1000–3000 Hz, and (*d*) envelope spectrum in the band 5000–6500 Hz

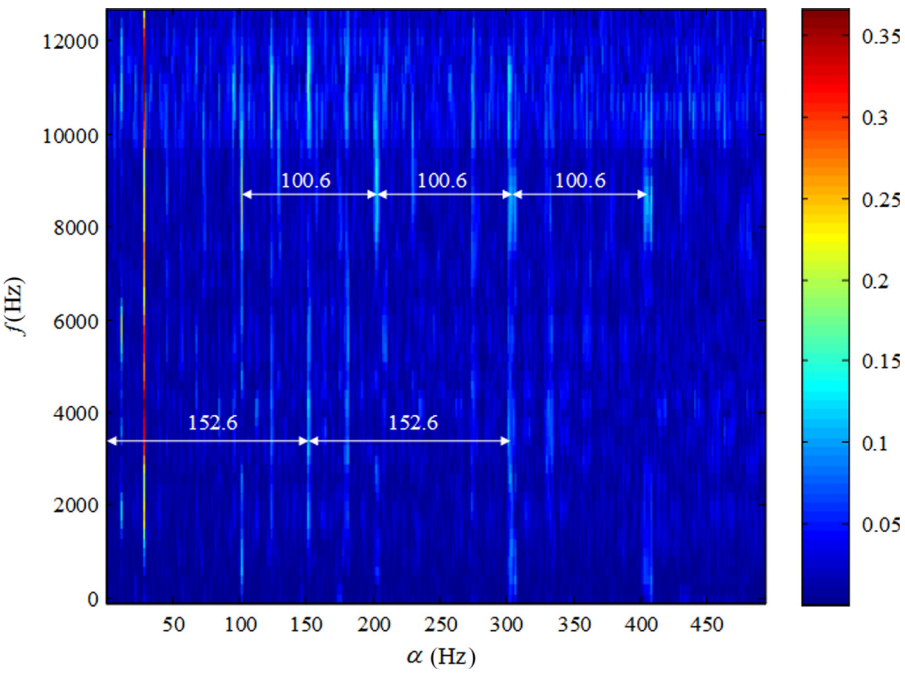

Fig. 4 Cyclic coherence function of the vibration signal

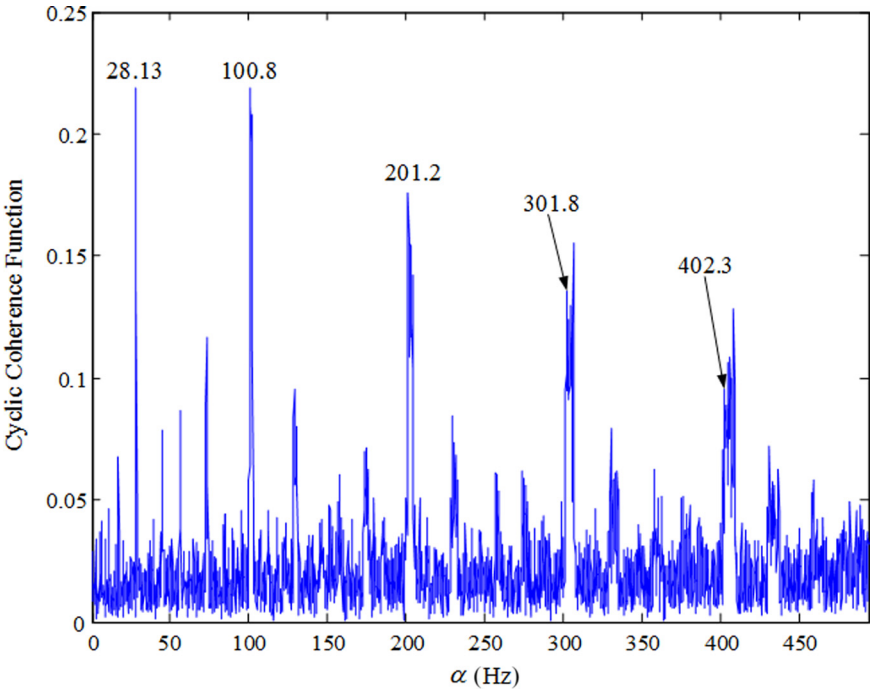

Fig. 5 Slice of CCF of the vibration signal at $f = 9000$ Hz

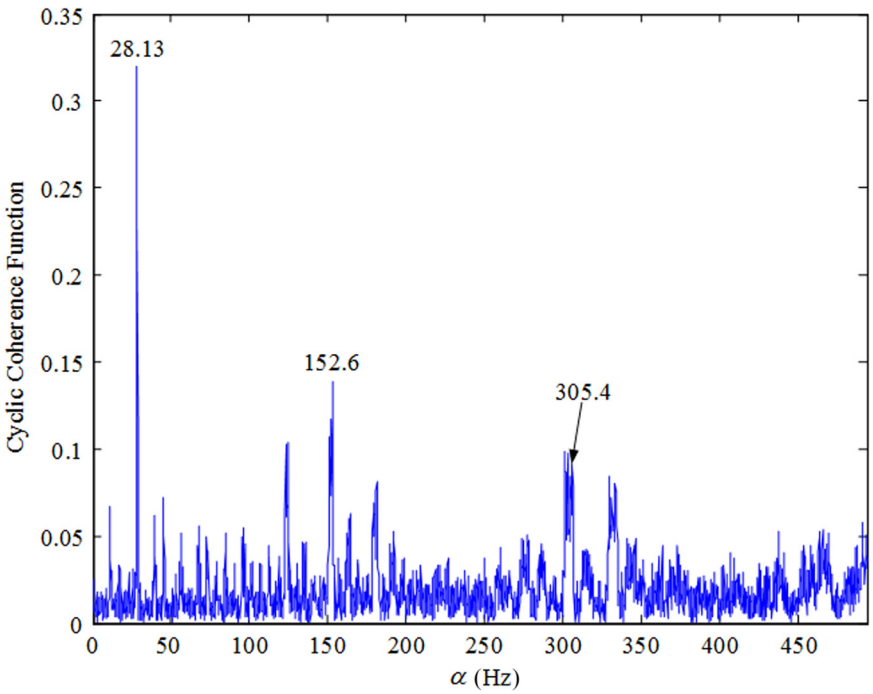

Fig. 6 Slice of CCF of the vibration signal at $f = 3500$ Hz

expression (1)–(4), the feature frequencies under the two conditions are listed in Table 1.

4.2 Test Results. A routine inspection has determined that the vibration level at the drive-end of the generator exceeded the VDI 3834 standard [30] value, as shown in Fig. 3(*a*). Figure 3(*b*) represents the corresponding power spectrum with the vibration energy concentrated in frequency bands from 1000 to 3000 Hz, and from 5000 Hz to 6500 Hz. A conventional approach for detecting bearing fault is to filter resonance frequency bands that may hide fault information, and get an envelope signal from demodulation analysis, e.g., Hilbert transform. The fault information can be evidenced by the analysis of the envelope spectrum (the Fourier transform of the envelope signal). Here fourth-order Butterworth band pass filters are designed to filter the original vibration signal at the above two frequency bands, and the envelope spectra of the filtered signal are shown as in Figs. 3(*c*)

Fig. 7 Disassembled bearing at the drive-end of the generator

and 3(*d*). The rotational frequency 28.13 Hz of the generator is evident. This may indicate an imbalance or a misalignment between generator's shaft and the high-speed shaft of the gearbox. In Figs. 3(*c*) and 3(*d*), there are components of 101.6 Hz (the second harmonic 203 Hz, the third harmonic 305 Hz) and 151.2 Hz (the second harmonic 302 Hz) present that are close to BPFO and BPFI in the third row of Table 1. These components may point to a fault on the inner or outer race of the bearing at the drive-end of generator. However, compared with the vibration amplitude of the rotational frequency (28.13 Hz) of the shaft, those of the BPFO (101.6 Hz) and BPFI (151.2 Hz) are weaker and can easily be ignored.

To explore possible faults of the bearing, the second-order cyclostationary analysis is adopted to process the original signal and the cyclic coherence function shown in Fig. 4. Besides of the rotational frequency of 28.13 Hz, there are regular intervals of 100.6 Hz and 152.6 Hz along the direction of the cyclic frequency axis in Fig. 4.

To improve computational efficiency of the cyclostationary analysis, the frequency resolution is low, and the resolution of cyclic frequency is high. All fault information is reflected in the cyclic frequency. Cyclic coherence function provides a three-dimensional representation in f–α plane for the vibration signal. The prominent components in CCF indicate their cyclostationarity, and therefore, each of them needs to be considered. By directly scanning the CCF, the fault modulation information along α axis can be detected. To find an optimal frequency that can slice the CCF to make an excellent exhibition of the fault feature, a ratio $C(f)$ between the amplitude ($C_{2x}^{\alpha_F}(f)$) of the BPFI (or BPFO, denoted by α_F) and the one ($C_{2x}^{\alpha_r}(f)$) of the rotational frequency denoted by α_r is defined as $C(f) = C_{2x}^{\alpha_F}(f)/C_{2x}^{\alpha_r}(f)$. The frequency corresponding to the maximal $C(f)$ is regarded as the optimal slice frequency.

From Fig. 4, BPFO (100.6 Hz) and its harmonics are concentrated at the frequency range from 8000 Hz to 10,000 Hz. And BPFI (152.6 Hz) and its harmonics are in the range from 2200 Hz to 4000 Hz. Figure 5 shows the optimal silce of CCF at $f = 9000$ Hz pointing to the BPFO feature frequency. At the same time, the silce of CCF at $f = 3500$ Hz in Fig. 6 indicates the feature frequency of BPFI. The above phenomena point to a fault at the inner and outer race of the bearing. The disassembled bearing from the drive-end of the generator in Fig. 7 confirms the diagnosis result.

The test data collected 6 months earlier from the same generator were used to validate the capability of cyclostationary analysis in detection of a faulty bearing. The original signal collected earlier is shown in Fig. 8(*a*) with the rotational frequency of the generator shaft of 24.84 Hz. The corresponding power spectrum is shown in Fig. 8(*b*). Similar to Fig. 3(*b*), the vibration energy concentrates in frequency band from 1000 to 3000 Hz, and from 5000 Hz to 6500 Hz. Figures 8(*c*) and 8(*d*) show the envelope spectra of the filtered signal at different frequency bands. Besides the rotational frequency (25 Hz and its harmonic) of the shaft, 269.5 Hz is evident, which is about twice the BPFI (134.38 Hz under condition C2). These phenomena illustrate that certain defects arose on the inner race of the bearing at that time. However, the BPFI itself is weak, and the BPFO does not appear in Figs. 8(*c*) and 8(*d*) comparing with Figs. 3(*c*) and 3(*d*), which demonstrate the enveloping demodulation analysis could not be effective.

The vibration signal in Fig. 8(*a*) collected 6 months earlier is processed by cyclostationary analysis. Its cyclic coherence function is shown in Fig. 9 where the BPFO intervals 89.8 Hz and BPFI 134.5 Hz are evident, coinciding with the feature frequency in the last row of Table 1. The slices at $f = 9000$ Hz and $f = 10{,}000$ Hz in Figs. 10 and 11 illustrate the fault features. The CCF from Figs. 9–11 illustrate that the bearing fault has emerged 6 months ago. Actually, this diagnosis was drawn at that time. However, since the fault hazard was not adequately assessed, the generator continued to operate, the faulty bearing had not been replaced until the later test at condition C1.

4.3 Comparison With Other Methods. To demonstrate the cyclostationarity of a faulty bearing in wind turbine generator, three methods of signal processing have been applied to compare the results from Figs. 9–11.

4.3.1 The Empirical Wavelet Transform. The empirical wavelet transform [31] is proposed to overcome the lack of theory of empirical mode decomposition. It can adaptively decompose signals into different modes by constructing multiple band-pass filters with parameters originating from the maxima in the frequency spectrum. Chen et al. [26] applied the empirical wavelet transform to detect a bearing fault of a wind turbine generator. Here, empirical wavelet transform is implemented based on the vibration signal in Fig. 8(*a*). The maximum number of frequency bands is set to three because three frequency bands can make a compromise between redundant detection and a good separation in power spectrum in this context. The result is shown in Fig. 12 where the left column illustrates the decomposed temporal modes, and the right column shows the corresponding envelope spectra. In mode 1, 89.84 Hz representing the BPFO is evident. The dominant frequency is 25 Hz in mode 2 and 3, which denotes the rotational frequency of shaft of the generator. In mode 3, there are 134.4 Hz and its second harmonic denoting the BPFI. Although

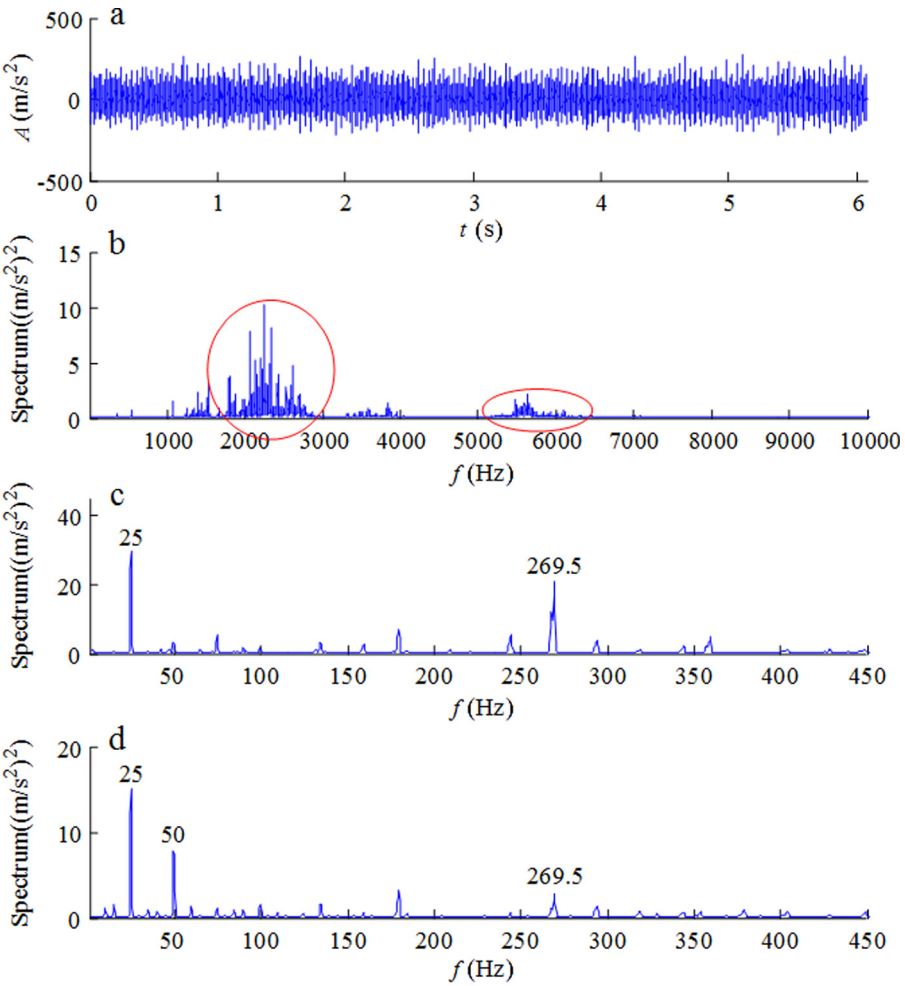

Fig. 8 Time signal 6 months earlier: (*a*) time signal, (*b*) power spectrum, (*c*) envelope spectrum in the band 1000–3000 Hz, and (*d*) envelope spectrum in the band 5000–6500 Hz

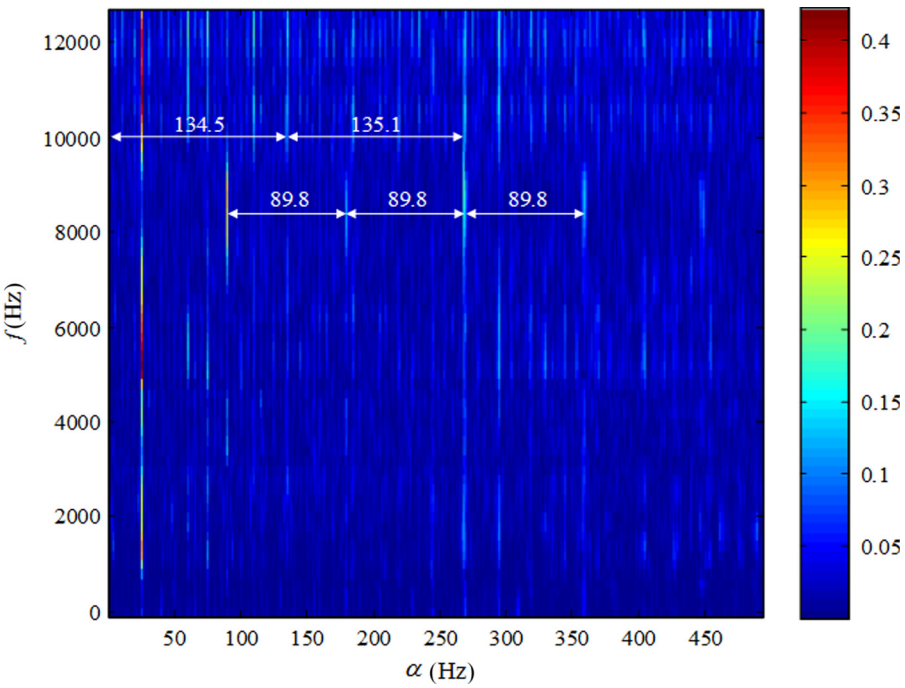

Fig. 9 Cyclic coherence function of the vibration signal 6 months earlier

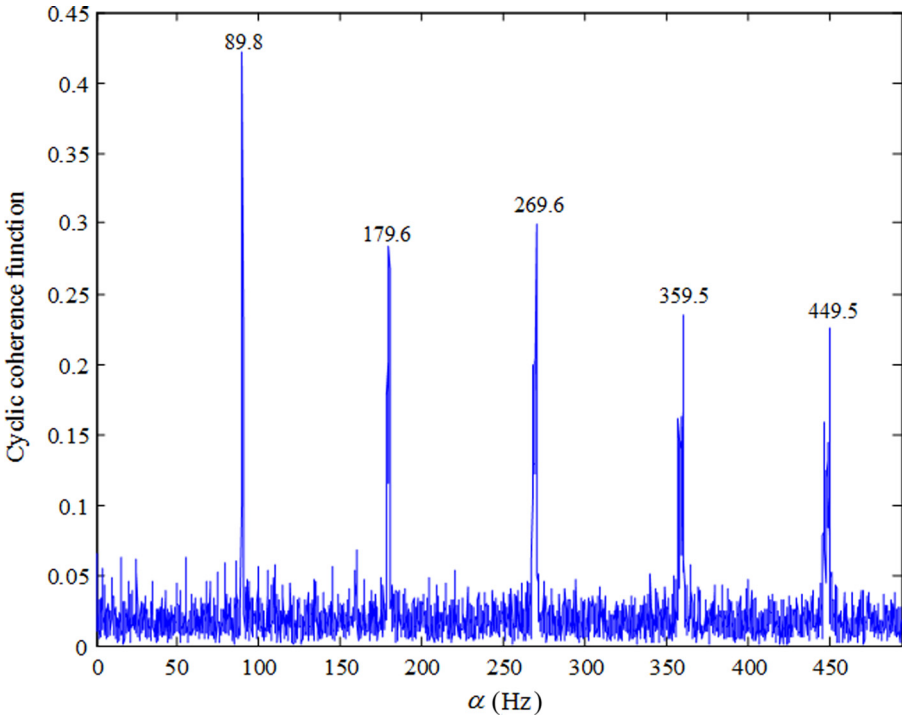

Fig. 10 Slice of CCF of the vibration signal 6 months earlier at $f = 9000$ Hz

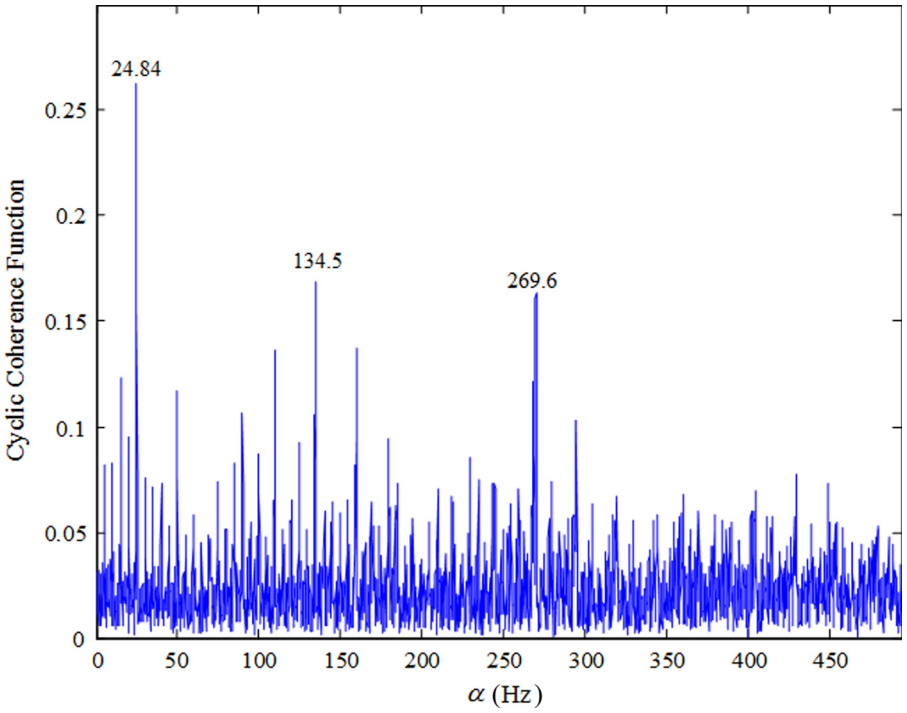

Fig. 11 Slice of CCF of the vibration signal 6 months earlier at $f = 10{,}000$ Hz

the BPFO is detected in mode 1 and the BPFI is detected in mode 3, they are less obvious than the slice of CCF in Fig. 10.

4.3.2 Morlet Wavelet Transform and Wigner–Ville Distribution. Tang et al. [27] adopted Morlet wavelet transform to denoise vibration signals and combined Wigner–Ville distribution to get a fault feature in time-frequency domain. The approach was verified in a wind turbine test-bed. Here, we used this approach to compare its performance with the second-order cyclostationary analysis.

First, the vibration signal 6 months earlier (see Fig. 8(*a*)) is processed based on the continuous Morlet wavelet transform shown in Fig. 13. The result illustrates that the effective frequencies are concentrated at the range from scale 6 to 11. Then, scale 9 is selected as the optimal parameter to filter the vibration signal. Using the smoothed pseudo Wigner–Ville distribution for the

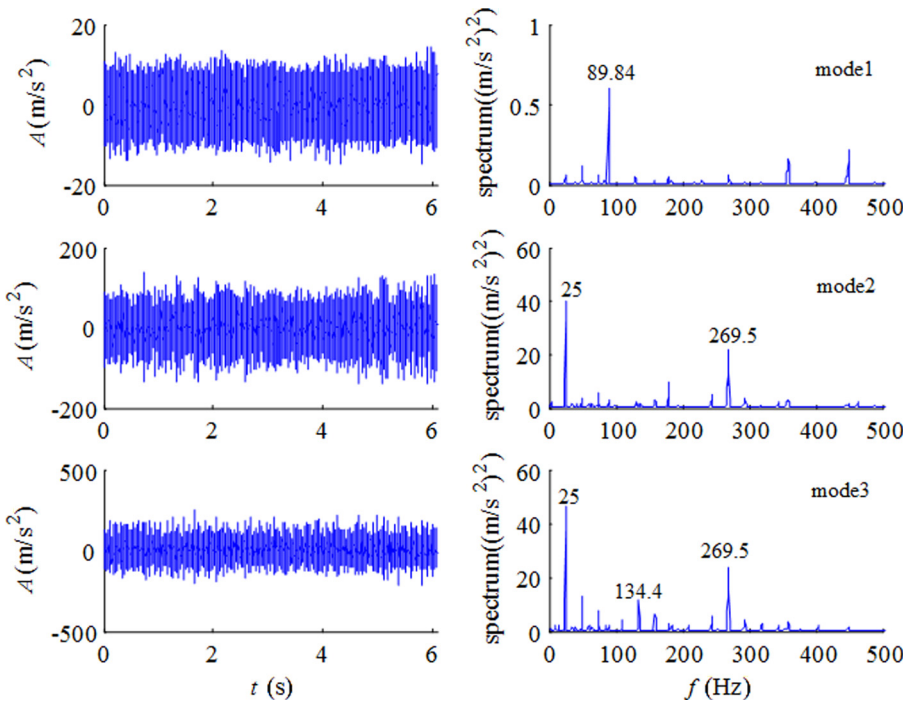

Fig. 12 Decomposed modes of empirical wavelet transform using the vibration signal 6 months earlier

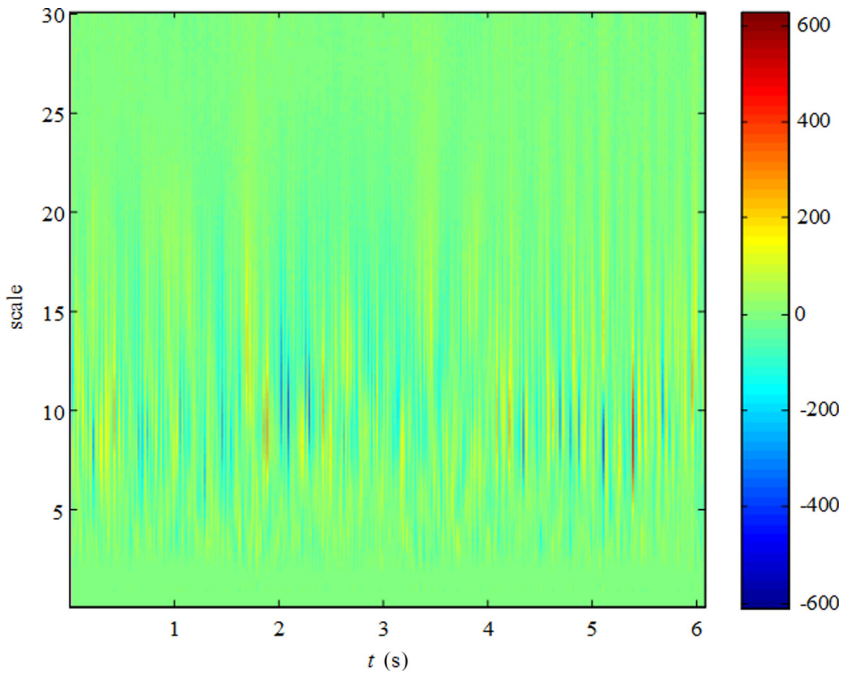

Fig. 13 The result produced by the continuous Morlet wavelet transform for the vibration signal 6 months earlier

filtered signal, the time-frequency representation is shown in Fig. 14 where only 0.04 s (25 Hz) denoting the rotational frequency of the shaft of the generator is distinct. The BPFI and BPFO do not appear. Performance of the second-order cyclostationary analysis is superior to the wavelet transform combined with Wigner–Ville distribution in detecting the bearing fault in wind turbine generator.

4.3.3 Short Time Fourier Transform. Short time Fourier transform is a time-frequency tool [29] to find the varying frequency in nonstationary signal. Window functions are used to separate the original signal into several parts, and the corresponding Fourier transforms are calculated. All the results from Fourier transforms are combined to form the time-frequency representation. Here, the length of window is 16,384 to make a compromise between the calculating efficiency and frequency resolution. Figure 15 is the STFT of the original signal 6 months earlier.

In Fig. 15, we can see the frequency components keep consistent, which demonstrates the wind turbine generator operated under a constant speed during the test. The vibration energy

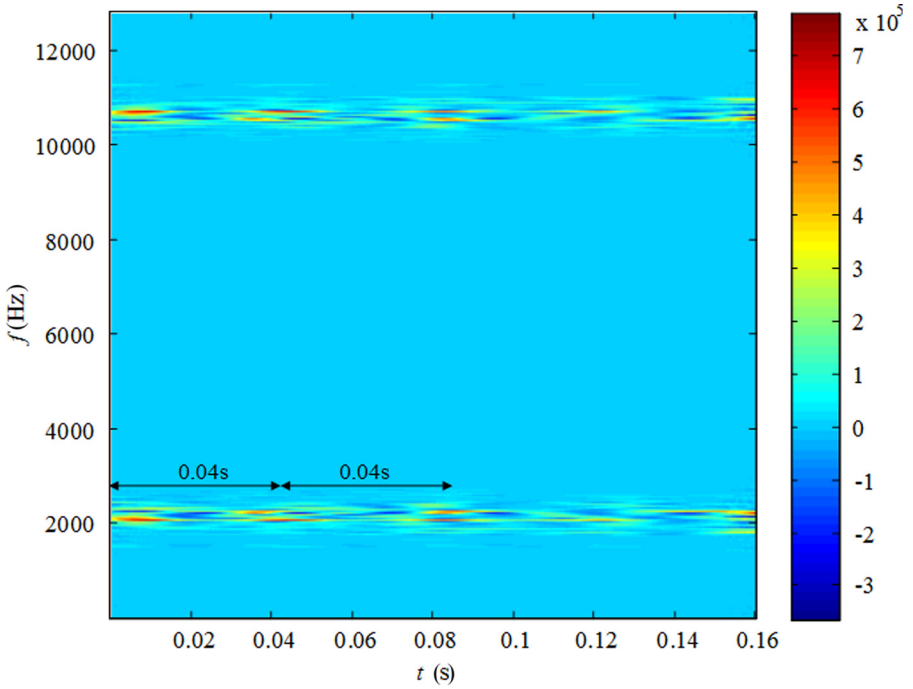

Fig. 14 Smoothed pseudo Wigner–Ville distribution of the filtered signal

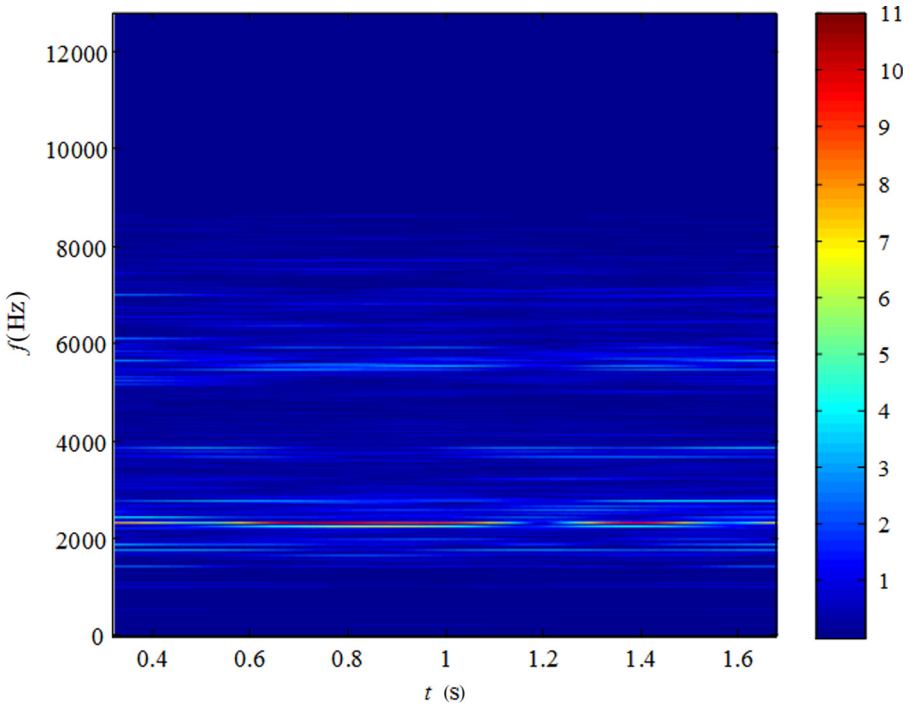

Fig. 15 Short time Fourier transform of the original signal 6 months earlier

concentrates on about 2300 Hz in time-frequency plane. The slice between 2000 Hz and 2800 Hz at $t = 1$ s is shown in Fig. 16. We can evidently see the frequency components 2068 Hz, 2158 Hz, 2248 Hz, 2338 Hz, and 2428 Hz with an interval 90 Hz denoting the BPFO. Also 2266 Hz, 2291 Hz, and 2316 Hz are manifested, with an interval 25 Hz denoting the rotational frequency of the shaft of the generator. Although the feature of the faulty bearing is detected using STFT, it still need an individual to identify the modulated sideband, thus is less direct than the cyclostationary analysis in Fig. 9.

4.4 Discussion. Observing the faulty bearing in Fig. 7, there are obvious traces of the current corrosion on the inner race caused by electric discharge of rotating parts. This is rather common phenomenon that may originate from the asymmetric

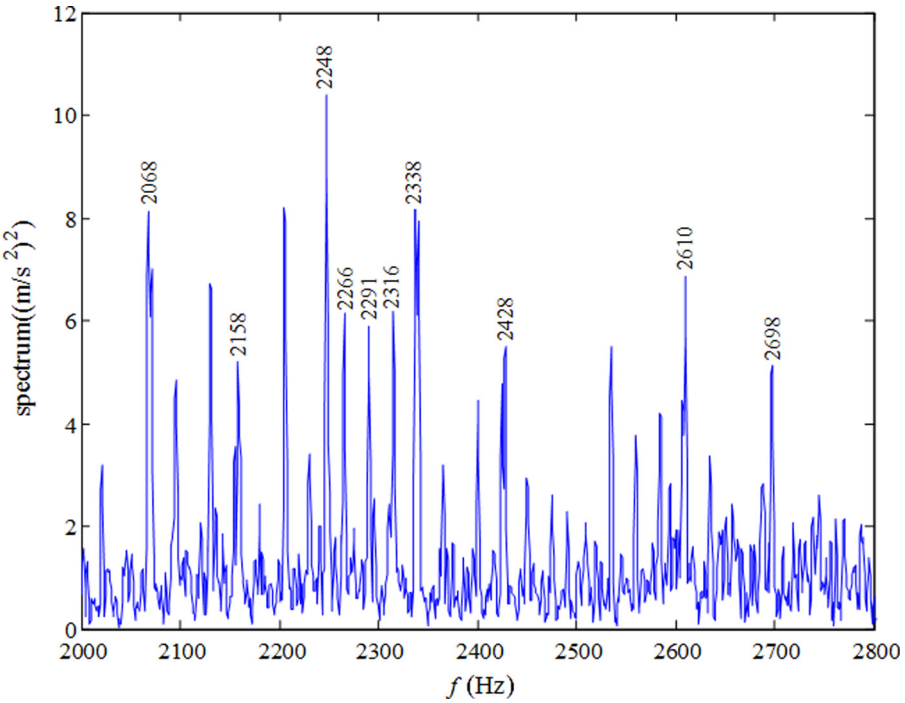

Fig. 16 The slice of STFT between 2000 Hz and 2800 Hz at $t = 1$ s

magnetic flux leakage, shaft eccentricity, or distorted grid current. Ground connection and proper lubrication of bearings are used to minimize discharge.

5 Conclusion

The research reported in the paper has demonstrated that cyclostationarity is a valuable characteristic in the analysis of bearing faults in the generator of a wind turbine. The second-order cyclostationary analysis was applied to the vibration signal from an industrial 1.5 MW wind turbine generator. The distinct fault frequency of the inner and outer race of a bearing was extracted.

The same analysis performed on the data collected 6 months earlier indicated emergence of the bearing fault at that time, which showed the ability of cyclostationary analysis to detect an incipient bearing fault. The diagnosis results were visualized with the disassembled bearing of a generator.

Acknowledgment

The research presented in this paper was supported by National Natural Science Foundation of China (Grant No. 51305135), Science and Technology Plan Projects of Hebei (Grant No. 15214307D), the Fundamental Research Funds for the Central Universities of China (Grant No. 2015ZD15), and the National High Technology Research and Development Program of China (863 Program) (Grant No. 2015AA043702).

References

[1] Amirat, Y., Benbouzid, M. E. H., Al-Ahmar, E., Bensaker, B., and Turri, S., 2009, "A Brief Status on Condition Monitoring and Fault Diagnosis in Wind Energy Conversion Systems," Renewable Sustainable Energy Rev., **13**(9), pp. 2629–2636.
[2] Marquez, F. P. G., Tobias, A. M., Perez, J. M. P., and Papaelias, M., 2012, "Condition Monitoring of Wind Turbines: Techniques and Methods," Renewable Energy, **48**, pp. 110–116.
[3] Wymore, M. L., Dam, J. E. V., Ceylan, H., and Qiao, D., 2015, "A Survey of Health Monitoring Systems for Wind Turbines," Renewable Sustainable Energy Rev., **52**, pp. 976–990.
[4] Alewine, K., and Chen, W., 2012, "A Review of Electrical Winding Failures in Wind Turbine Generators," IEEE Electr. Insul. Mag., **28**(4), pp. 8–13.
[5] Tavner, P. J., 2008, "Review of Condition Monitoring of Rotating Electrical Machines," IET Electr. Power Appl., **2**(4), pp. 215–247.
[6] Watson, S. J., Xiang, B. J., Yang, W. X., Tavner, P. J., and Crabtree, C. J., 2010, "Condition Monitoring of the Power Output of Wind Turbine Generators Using Wavelets," IEEE Trans. Energy Convers., **25**(3), pp. 715–721.
[7] Kusiak, A., and Verma, A., 2012, "Analyzing Bearing Faults in Wind Turbines: A Data-Mining Approach," Renewable Energy, **48**(6), pp. 110–116.
[8] Yang, W. X., Court, R., and Jiang, J. S., 2013, "Wind Turbine Condition Monitoring by the Approach of SCADA Data Analysis," Renewable Energy, **53**(9), pp. 365–376.
[9] Antoni, J., and Randall, R. B., 2006, "The Spectral Kurtosis: Application to the Vibratory Surveillance and Diagnostics of Rotating Machines," Mech. Syst. Signal Process., **20**(2), pp. 308–331.
[10] Li, R., Sopon, P., and He, D., 2012, "Fault Features Extraction for Bearing Prognostics," J. Intell. Manuf., **23**(2), pp. 313–321.
[11] Sawalhi, N., Randall, R. B., and Endo, H., 2007, "The Enhancement of Fault Detection and Diagnosis in Rolling Element Bearings Using Minimum Entropy Combined With Spectral Kurtosis," Mech. Syst. Signal Process., **21**(6), pp. 2616–2633.
[12] Randall, R. B., Sawalhi, N., and Coats, M., 2011, "A Comparison of Methods for Separation of Deterministic and Random Signals," Int. J. Cond. Monit., **1**(1), pp. 11–19.
[13] Borghesani, P., Pennacchi, P., Randall, R. B., Sawalhi, N., and Ricci, R., 2013, "Application of Cepstrum Pre-Whitening for the Diagnosis of Bearing Faults Under Variable Speed Conditions," Mech. Syst. Signal Process., **36**(2), pp. 370–384.
[14] Rai, V. K., and Mohanty, A. R., 2007, "Bearing Fault Diagnosis Using FFT of Intrinsic Mode Functions in Hilbert–Huang Transform," Mech. Syst. Signal Process., **21**(6), pp. 2607–2615.
[15] Park, C. S., Choi, Y. C., and Kim, Y. H., 2013, "Early Fault Detection in Automotive Ball Bearings Using the Minimum Variance Cepstrum," Mech. Syst. Signal Process., **38**(2), pp. 534–548.
[16] Teng, W., Jiang, R., Ding, X., Liu, Y. B., and Ma, Z. Y., 2016, "Detection and Quantization of Bearing Fault in Direct Drive Wind Turbine Via Comparative Analysis," Shock Vib., **2016**(2), pp. 1–12.
[17] Dandawate, A. V., and Giannakis, B. G., 1994, "Statistical Tests for Presence of Cyclostationary," IEEE Trans. Signal Process., **42**(9), pp. 2355–2368.
[18] He, Z. J., Zi, Y. Y., and Zhang, X. N., 2007, *Modern Signal Processing and Its Application in Engineering*, Xi'an Jiaotong University Press, Xi'an, China.
[19] Gardner, W. A., 1991, "Exploitation of Spectral Redundancy in Cyclostationary Signals," IEEE Signal Process. Mag., **8**(2), pp. 14–36.
[20] Gardner, W. A., 1986, "Measurement of Spectral Correlation," IEEE Trans. Acoust., Speech, Signal Process., **34**(5), pp. 1111–1123.
[21] Gardner, W. A., 1986, "The Spectral Correlation Theory of Cyclostationary Time-Series," Signal Process., **11**(1), pp. 13–36.
[22] Antoni, J., Bonnardot, F., Raad, A., and Badaoui, M. E., 2004, "Cyclostationary Modelling of Rotating Machine Vibration Signals," Mech. Syst. Signal Process., **18**(6), pp. 1285–1314.
[23] Antoni, J., 2007, "Cyclic Spectral Analysis in Practice," Mech. Syst. Signal Process., **21**(2), pp. 597–630.

[24] Antoni, J., 2007, "Cyclic Spectral Analysis of Rolling-Element Bearing Signals: Facts and Fictions," J. Sound Vib., **304**(3–5), pp. 497–529.
[25] Raad, A., Antoni, J., and Sidahmed, M., 2008, "Indicators of Cyclostationarity: Theory and Applications to Gear Fault Monitoring," Mech. Syst. Signal Process., **22**(3), pp. 574–587.
[26] Chen, J., Pan, J., Li, Z., Zi, Y., and Chen, X., 2016, "Generator Bearing Fault Diagnosis Via Empirical Wavelet Transform Using Measured Vibration Signals," Renewable Energy, **89**, pp. 80–92.
[27] Tang, B., Liu, W., and Song, T., 2010, "Wind Turbine Fault Diagnosis Based on Morlet Wavelet Transformation and Wigner–Ville Distribution," Renewable Energy, **35**(12), pp. 2822–2866.
[28] Zhang, X. D., and Bao, Z., 1998, *Nonstationary Signal Analysis and Processing*, National Defense Industry Press, Beijing, China.
[29] Allen, J. B., 1977, "Short Time Spectral Analysis, Synthesis, and Modification by Discrete Fourier Transform," IEEE Trans. Acoust., Speech, Signal Process., **25**(3), pp. 235–238.
[30] VDI 3834, 2009, "Measurement and Evaluation of the Mechanical Vibration of Wind Energy Turbines and Their Components Onshore Wind Energy Turbines With Gears," Verlag des Vereins Deutscher Ingenieure, p. 16.
[31] Gilles, J., 2013, "Empirical Wavelet Transform," IEEE Trans. Signal Process., **61**(16), pp. 3999–4010.